SynOpen S. Prakash et al. THIEME OPEN ACCESS Paper

Gum Acacia Stabilized Ag-TiO_2 and Ag-SiO_2: Sustainable Nanocatalysts for Direct and Convenient Synthesis of 5-Substituted 1*H*-tetrazoles

Supriya Prakash[*a]
Bojja Sreedhar[b]
N. V. S. Naidu[c]

[a] Department of Chemistry, Gokaraju Rangaraju Institute of Engineering and Technology, Hyderabad-500090, India
drsupriya2309@gmail.com
[b] Inorganic and Physical Chemistry Division, CSIR-Indian Institute of Chemical Technology, Hyderabad-500007, India
sreedharb@iict.res.in
[c] Department of Chemistry, Sri Venkateswara University, Tirupati-517501, India
nvsn69@gmail.com

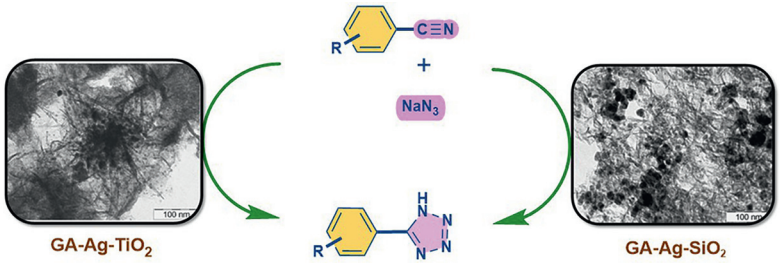

Received: 07.08.2023
Accepted after revision: 18.08.2023
Published online: 23.11.2023 (Version of Record)
DOI: 10.1055/s-0042-1751511; Art ID: SO-2023-08-0062-OP

Abstract We describe the use of biocompatible gum acacia (GA)-assembled Ag-TiO_2 and Ag-SiO_2 nanostructures as effective heterogeneous catalysts for the synthesis of 5-substituted 1*H*-tetrazoles through the traditional [3+2] cycloaddition of aryl nitriles with sodium azides. Characterization of the prepared catalysts employing TEM, XPS, FE-SEM, FT-IR, XRD, and TGA-DTG reveals silver nanoparticles encapsulated in the GA matrix amidst modified nano titania or silica. A variety of structurally divergent aryl nitriles were converted into the corresponding tetrazoles in a short reaction time. Other advantages include low catalytic load, easy handling of catalyst, limited use of toxic reagents, and desirable conversion yields, making this protocol a viable and practical alternative for this cyclization. The catalysts can be easily recovered and reused over multiple cycles without significant loss of catalytic activity.

Key words nanohybrids, biocomposites, 5-substituted 1*H*-tetrazoles, gum acacia, silver nanoparticles

Bio-based methods offer a greener option for manageable construction of nanomaterials with limited environmental impact. Nanocatalysts prepared using these methods are not only chemically stable and biodegradable but also exhibit excellent catalytic activity.[1–4] One such conventional method of acquiring nanostructured materials is biomimetic synthesis, which is a classic, versatile, and cost-effective strategy.[5] This template-assisted synthetic route has been extensively studied as an alternate and dynamic approach for the preparation of nanomaterials that minimizes the use of toxic substances in synthesis.[6,7] Furthermore, the scaffolding provided by the bio-based templates for assemblage of inorganic materials facilitates direct aqueous-phase synthesis of nanoparticles, making it a promising approach for large-scale production of various nanomaterials.[8–13] Gum acacia (GA), a natural gum exudate, is one such model that consists of a highly branched polysaccharide acid mixture composed of carbohydrate moieties and a small portion of hydroxyl proline-rich protein. The intrinsic, innocuous, and bio-congruous properties of GA have made it a promising stabilizer, dispersant, and significant crystal growth modifier, as well as a powerful reductant for the synthesis of a variety of nanoparticles.[14–18]

Over the years, the nanomaterials have proven to be one of the most convenient and powerful categories of heterogeneous catalysts, and they have found numerous synthetic and catalytic applications.[19–21] One significant challenge for the research community has been to develop new catalysts that can operate under ambient conditions while offering a high degree of selectivity for functional groups. With a view to developing potential nanocomposites, the catalysts are generally employed in the form of nanocomposites in which the active metal species are dispersed onto support materials such as polymers, carbon materials, mesoporous materials, metal oxides, resins, or inorganic porous materials.[22–27] This facilitates recycling of the nanocomposites and makes them extremely economical and beneficial for industrial applications.

Supported silver nanoparticles[28] have generated a great deal of interest in the field of synthetic organic chemistry for their outstanding catalytic activity, and they have been employed extensively as heterogeneous catalysts in a variety of chemical transformations, including coupling, cycloaddition, reduction, oxidation, and asymmetric synthe-

sis.[29–36] The remarkable catalytic activity of supported silver nanoparticles is attributed to uniform dispersion, high surface area, quantum-size effects, limited tendency of aggregation, improved chemical stability, synergistic effect of the support, particle size, and oxidation state of the silver metal.

Tetrazoles represent a substantial group of synthetic heterocyclic organic compounds, with a five-membered ring comprised of four nitrogen atoms and one carbon atom.[37,38] These nitrogen-rich ring systems have gathered recognition on account of their wide utility in a variety of synthetic, medicinal, and especially pharmaceutical applications, and they exhibit strong activities such as anticancer, antifungal, antimicrobial, antihypertensive, antiallergic, and analgesic properties.[39–45] Their implementation has been extended to agriculture as herbicides, fungicides,[46] and potential plant-growth regulators,[47] and further to material science in areas such as explosives, propellants, and photography.[48–50]

Although construction of the tetrazole ring can be achieved in a variety of ways and several new approaches as well as modifications of established methods have emerged, synthesizing 5-substituted 1*H*-tetrazoles has consistently been challenging. The most convenient route is considered to be the cycloaddition of the azide moiety to the corresponding aryl nitriles employing diverse catalysts under various solvent conditions.[51] In this connection, many homogeneous[52–55] and heterogeneous pathways[56–58] have been communicated.

Among the various nanocatalysts previously reported for synthesizing tetrazole derivatives, silver nanoparticles have received less attention.[59,60] The use of toxic and harsh reagents in nanoparticles synthesis, challenges in recovery of the catalyst due to agglomeration of nanoparticles, leaching of metal during reaction, high catalytic load, and long reaction times suggest that there is scope for improvising these processes to simplify synthesis and minimize or avoid their individual drawbacks.

Herein, we report the use of bio-regulated, conveniently recyclable, hydrothermally synthesized gum acacia-assisted Ag-TiO_2 and Ag-SiO_2 nanocomposites for the successful synthesis of 5-substituted 1*H*-tetrazoles by the [3+2] cycloaddition of aryl nitriles with sodium azide. The presence of modified TiO_2 or SiO_2 not only imparts distinctive structures to nanocatalysts but also enhances their catalytic surface area. This improvement facilitates the catalytic processes and prevents catalyst poisoning during reaction, leaving behind residue-free products.

Structural, chemical, morphological, and thermal analyses of GA-Ag-TiO_2 and GA-Ag-SiO_2 nanocomposites were conducted using XRD, XPS, FT-IR, TEM, FE-SEM, and TGA-DTG techniques.

XRD Analysis

X-ray diffraction patterns of the obtained GA-Ag-TiO_2 and GA-Ag-SiO_2 before and after catalysis are illustrated in Figure 1 and Figure 2, respectively. The XRD spectrum of GA-Ag-TiO_2 (Figure 1) features four characteristic diffraction peaks at 2θ = 38.24, 44.36, 64.69, and 77.49° corresponding to planes (111), (200), (220), and (311), respectively, and can be assigned well to the face-centered cubic structure of silver metal (JCPDS card No. 4-783). The additional peaks at 2θ = 25.4, 54.5, 62.5, and 75.0° with orientations (101), (105), (204), and (215), respectively, can be attributed to anatase TiO_2 (JCPDS card No. 21-1272).[61] The average crystallite size of Ag and TiO_2 nanoparticles as determined from the full-width half-maximum (FWHM) of the characteristic peak value in the Debye–Scherer equation was found to be 20.9 and 18.2 nm, respectively.

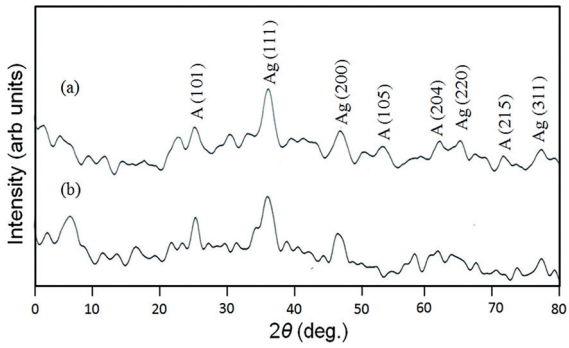

Figure 1 XRD spectrum of GA-Ag-TiO_2 (a) as-prepared catalyst, and (b) recycled catalysts after five subsequent reuses.

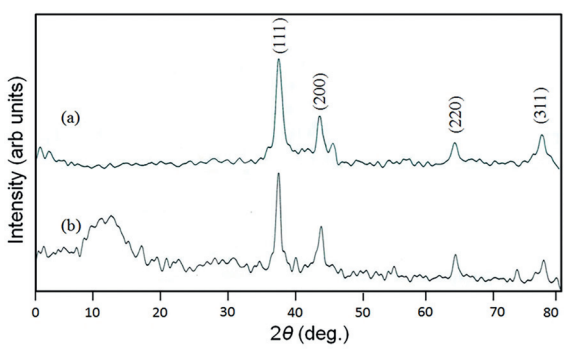

Figure 2 XRD spectrum of GA-Ag-SiO_2 (a) as-prepared catalyst, and (b) recycled catalysts after five subsequent reuses.

Similarly, the XRD spectrum of GA-Ag-SiO_2 (Figure 2) displays all the typical characteristic peaks of highly crystalline FCC silver (JCPDS card No. 4-783).[62,63] The average crystallite size of Ag nanoparticles in this nanocatalyst was calculated to be 24.8 nm.

The XRD spectra of recycled catalysts (Figure 1b and Figure 2b) are consistent with those of fresh catalysts and exhibit no significant transformation with respect to crystallinity, orientation, or phase of nanoparticles, clearly indicating the durability of the catalysts.

TEM Study

Transmission electron microscopy (TEM) images of as-prepared nanocatalysts facilitate the understanding of the structure, size, and dispersion of silver nanoparticles on their respective supports. In case of GA-Ag-TiO_2 (Figure 3), distended dark Ag nanoparticle aggregates were identified that were dispersed on the network of gum acacia. The pale fringes and murky centers clearly suggest the presence of silver nanoparticles enriched on the nanoplate of GA assembled TiO_2.

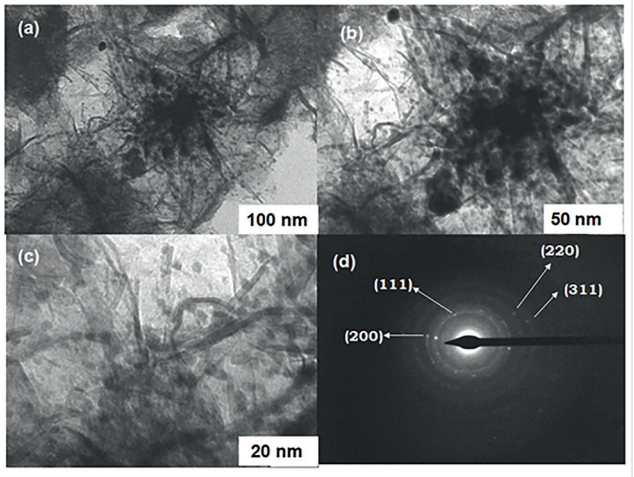

Figure 3 TEM images of fresh GA-Ag-TiO_2 (a) at lower magnifications, (b,c) at higher magnifications, and (d) SAED pattern.

The selected area electron diffraction (SAED) pattern (Figure 3d) displayed a few bright spots (111), (200), (220), and (311) that correspond to crystalline silver.[64] Analogous TEM studies of GA-Ag-SiO_2 (Figure 4) revealed a considerable number of silver nanoparticles present on the matrix of GA amidst amorphous SiO_2. The SAED pattern in Figure 4d included well-resolved rings corresponding to highly crystalline silver metal.[64]

TEM analysis of the recycled catalysts (see the Supporting Information) showed no significant differences compared to new catalysts, which strongly supports the efficacy of these catalysts in delivering consistent yields during subsequent cycles.

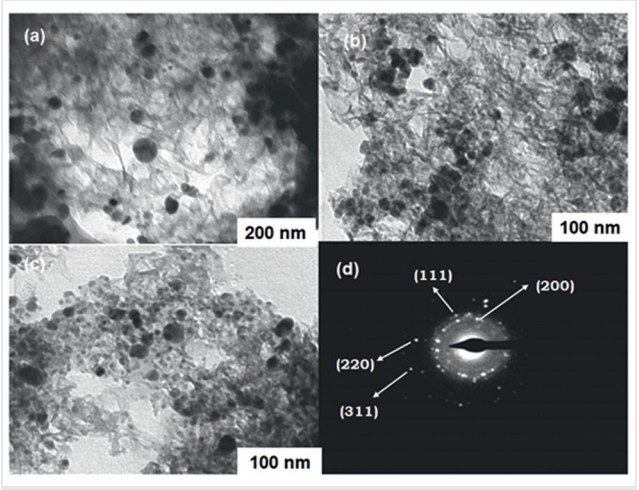

Figure 4 TEM images of fresh GA-Ag-SiO_2 (a) at lower, (b,c) at higher magnifications, and (d) SAED pattern.

TG-DTG Analysis

The thermal stability and decomposition profile of the GA-Ag-TiO_2 and GA-Ag-SiO_2 nanocatalysts were demonstrated using thermogravimetric analysis in the temperature range from 25 to 1000 °C at a heating rate of 20 °C/min under N_2 atmosphere. The thermogram of GA-Ag-TiO_2 (Figure 5) exhibits an initial small weight-reduction step between 40 and 140 °C (weight loss of 5.6%), representing the elimination of physiosorbed water from the saccharide framework. The following minor decomposition step occurs at 185–225 °C (weight loss of 1.2%) and is attributed to the expulsion of trapped water and CO_2 from the pores of the material.

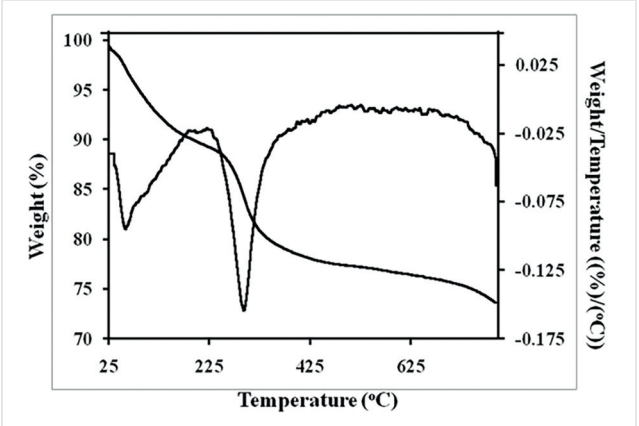

Figure 5 Thermogram of as-prepared GA-Ag-TiO_2

Table 1 TGA/DTG Analysis of As-Prepared GA-Ag-TiO_2 and GA-Ag-SiO_2 Nanocomposites

Sample	Decomp. phase	Temp. range (°C)	Weight loss (%)
GA-Ag/TiO_2	1	40–140	5.6
	2	185–225	1.2
	3	235–375	18.2
GA-Ag/SiO_2	1	35–140	2.6
	2	160–225	1.4
	3	245–400	5.8

The next significant step in the decomposition process takes place at 235–375 °C (weight loss of 18.2%), corresponding to the breakdown of various organic moieties, such as –OH and –COOH, present in GA.

Similarly, the thermogram of GA-Ag-TiO_2 (Figure 6) exhibits a three-stage decomposition pattern with lower percentages of weight loss. An initial minor decomposition phase (weight loss of 2.6%) occurring at 35–140 °C indicates the loss of structural water. The subsequent decomposition phases at 160–225 °C (weight loss of 1.4%) and 245–400 °C (weight loss of 5.8%), respectively, are the consequence of deconstruction of various components of GA. Previously established by our TGA-MS studies, the evolution of CO_2 during these decomposition stages results from the breakdown of –COOH functional groups found in GA, indicating that these nanostructures are inorganic–organic hybrid materials.[65–67]

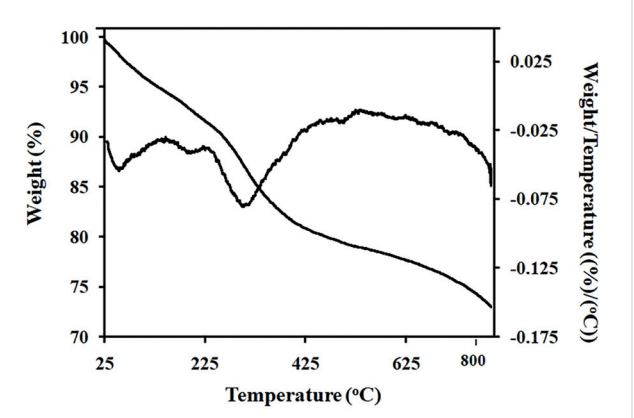

Figure 6 Thermogram of as-prepared GA-Ag-SiO_2

As observed in Table 1, both catalysts can withstand heat deterioration, especially in the early phases between 25 and 225 °C, with only physiosorbed water loss. This emphasizes their stability and resilience, especially under high-temperature reaction settings.

XPS Analysis

The chemical composition and status of as-prepared GA-Ag-TiO_2 and GA-Ag-SiO_2 nanocomposites were assessed using X-ray photoelectron spectroscopy, as presented in Figure 7 and Figure 8, respectively. The existence of relevant elements in each nanocatalyst was demonstrated with the survey scan spectra of respective nanocomposites.

As seen in Figure 7a, the peaks corresponding to C 1s (282.9 eV), N 1s (397.1 eV), O 1s (527.7 eV), Ti 2p (456.1 eV), and Ag 3d (368.1 eV) represent C, N, O, Ti, and Ag, respectively, in GA-Ag-TiO_2 nanocomposite. Similarly, as seen in Figure 8a, the peaks corresponding to C 1s (284.6 eV), N 1s (398.1 eV), O 1s (532.4 eV), Si 2p (103.3 eV), and Ag 3d (368.4 eV) represent C, N, O, Si, and Ag, respectively, in GA-Ag-SiO_2 nanocomposite. The elements C, N, and O correspond to –NH_2 and –COOH groups of amino acid residues present in GA. The deconvolution of high-resolution narrow scans of C 1s Figure 7b and Figure 8b reveal four components that are characteristic of various substituted carbon moieties present in GA. Our prior investigations confirmed these findings.[65,66]

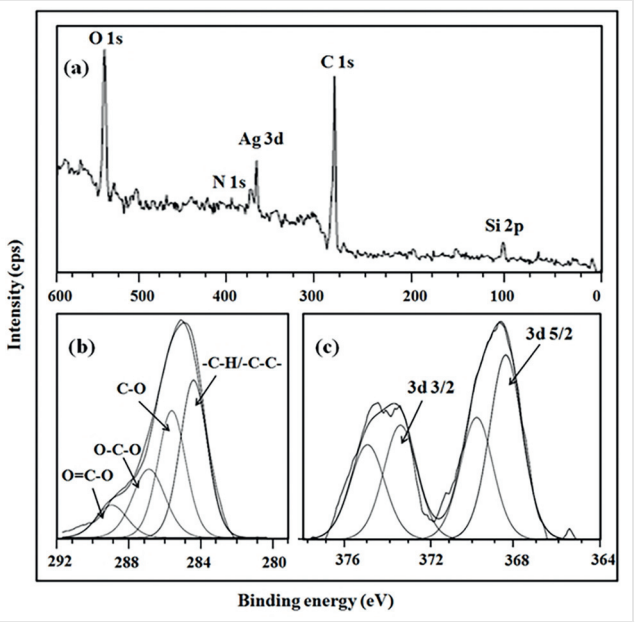

Figure 7 GA-Ag-TiO_2 X-ray photoelectron spectroscopy. (a) Survey scan spectrum, and high-resolution narrow scans of (b) C 1s and (c) Ag 3d.

As observed in Figure 7c and Figure 8c, the Ag 3d spectra of both nanocatalysts show a major contribution followed by a minor component at higher binding energy (BE) values. The acquired spectra could be deconvoluted to two sets of two peaks, with first set at ca. 368 and ca. 374 eV attributable to metallic silver and second set at ca. 370 and ca. 376 eV due to Ag(II) species.

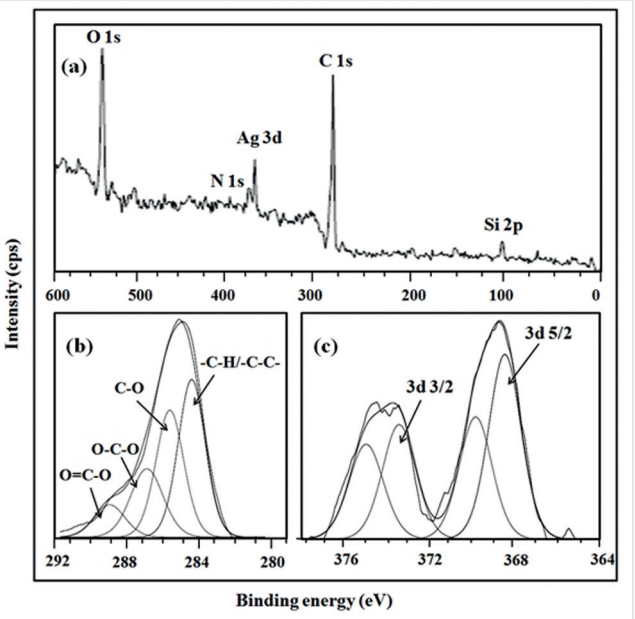

Figure 8 GA-Ag-SiO_2 X-ray photoelectron spectroscopy. (a) Survey scan spectrum, and high-resolution narrow scans of (b) C 1s and (c) Ag 3d.

Despite the existence of silver in two oxidation states visible in both spectra, the higher intensities for silver effectively indicated that the majority of the deposited silver is in its metallic form, while the remaining quantity represents the unreduced ionic species emerging from the silver Ag precursor, that eventually form the surface capping of the nanocatalyst.[68] The results are in good agreement with a previous report.[69]

FE-SEM Study

FE-SEM images of both catalysts reveal a considerable quantity of silver nanoparticles mainly deposited over the surface of the host matrix (GA); upon closer inspection, it is seen that smaller silver nanoparticles are disseminated within the inner layers. In case of GA-Ag-TiO_2 (Figure 9), the nanoparticles have a nearly spherical form and exhibit aggregation of particles along the boundaries of TiO_2 grains. In contrast, GA-Ag-SiO_2 (Figure 10) shows an irregular sponge-like network of particles with increased coalescence. This unusual and disorganized configuration is characteristic of the synthetic strategy used, which justifies the simplistic separation of the catalysts.

The comparable TEM images showed similar morphologies.

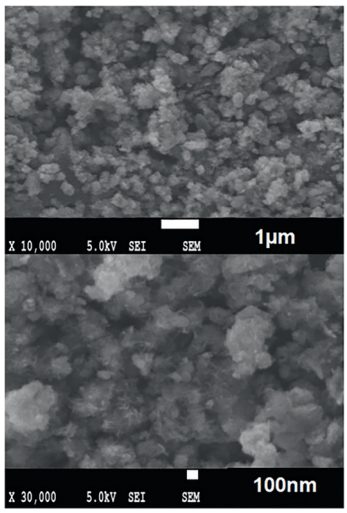

Figure 9 FE-SEM images of as-prepared GA-Ag-TiO_2 at (a) lower and (b) higher magnification.

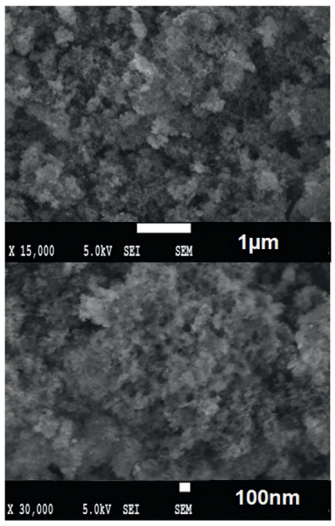

Figure 10 FE-SEM images of as-prepared GA-Ag-SiO_2 at (a) lower and (b) higher magnification.

FT-IR Analysis

To study the potential interaction of formed silver nanoparticles with their respective supports and to evaluate their steric stabilization via functional groups of GA, FT-IR spectra of catalysts were recorded (Figure 11). When the acacia functional groups adhere to the nanoparticles' surface, the corresponding stretching frequencies of functional groups present in acacia (Figure 11a) were expected to shift accordingly.[70] As can be seen with GA-Ag-TiO_2 (Figure 11b), the peaks of GA corresponding to stretching vibration of –OH, shifted to 3378.10 cm^{-1}, the symmetric stretching and bending vibrations of $-CH_2-$ shifted to 2927.15 cm^{-1} and 1068.27 cm^{-1}, respectively, and C=O stretching and–OH bending of the acid group shifted to 1610.02 cm^{-1} and

1417.62 cm^{-1}, respectively. A distinctive band related to stretching of TiO group was observed at 470.84 cm^{-1}, corresponding TiO_2 nanoparticles in the catalyst.[71]

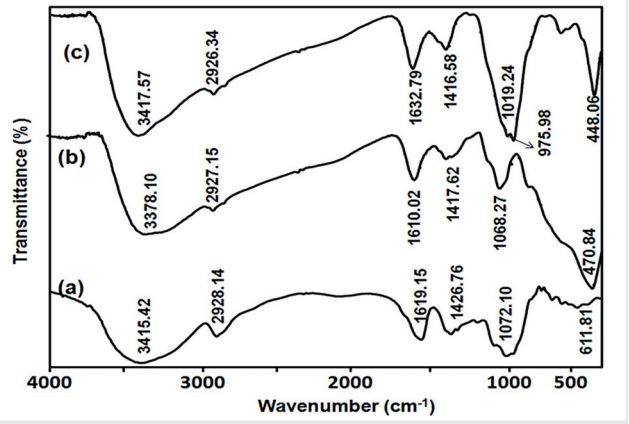

Figure 11 FT-IR spectra of (a) gum acacia (b) as-prepared GA-Ag-TiO_2, and (c) GA-Ag-SiO_2 nanocomposites

In GA-Ag-SiO_2 (Figure 11c), the peaks of GA corresponding to the stretching vibration of –OH, shifted to 3417.57 cm^{-1}, the symmetric stretching and bending vibrations of –CH_2– shifted to 2926.34 cm^{-1} and 1032.79 cm^{-1}, respectively, and C=O stretching and –OH bending of the acid group shifted to1632.79 cm^{-1} and 1416.58 cm^{-1}, respectively. The characteristic absorption bands at 975.98, 663.43, and 448.06 cm^{-1} represent the symmetric stretching, in-plane bending, and rocking mode vibrations, respectively, of the Si-O-Si group of silica.[72] These findings provide clear evidence of the steric stabilization of nanoparticles by gum acacia molecules, providing effective surface passivation (through interactions with –COOH and –OH groups), thereby preventing nanoparticle aggregation in the system.[65–67]

Evaluation of Catalytic Activity of GA-Ag-TiO_2 and GA-Ag-SiO_2 Nanocomposites

The catalytic efficacy of the as-prepared nanocomposites was studied for the synthesis of 5-substituted 1*H*-tetrazoles via [3+2] cycloaddition of aryl nitrile and sodium azide. Conventionally, cycloadditions require high temperatures, sometimes as high as 130 °C, but most organic solvents are sensitive to these temperatures. Therefore, DMF and DMSO are considered solvents that are well-suited for such reactions.[73–75] DMF was selected for further optimization studies involving different catalysts and catalytic amounts (Table 2) as it is easily removable and allows for smooth recovery of the catalyst. An increase in the amount of catalyst significantly improved the percentage yield, which could be attributed to the presence of an increased number of active catalyst sites.

Table 2 Optimization of Catalyst and Catalytic Amounts for the Synthesis of Tetrazoles[a]

Entry	Catalyst	Catalyst load (mg)	Time (h)	Yield (%)[b]
1	GA-Ag-TiO_2	25	12	38
	GA-Ag-SiO_2	25	12	40
2	GA-Ag-TiO_2	50	12	51
	GA-Ag-SiO_2	50	12	56
3	GA-Ag-TiO_2	100	5	84
	GA-Ag-SiO_2	100	5	87
4	GA-Ag-TiO_2	200	12	85
	GA-Ag-SiO_2	200	12	89
5	nano GA-Ag	100	12	61
	GA-TiO_2	100	24	8
	GA-SiO_2	100	24	0

[a] Reaction conditions: Phenyl nitrile (1 mmol), NaN_3 (1.5 mmol) in DMF at 120 °C.
[b] Isolated yield.

This optimized catalytic system was then assessed for its scope and limitations using a series of aryl nitriles with differing steric characteristics and with a range of functional groups at differing positions on the aromatic ring (Table 3). Notably, aryl nitriles bearing halogen atoms afforded desirable yields, as the halogen atom remained unaffected by the process (entries 2–4). This provides the possibility for further functionalization of the resulting tetrazole product.

The overall results demonstrate the convincing catalytic activity of GA-Ag-TiO_2 and GA-Ag-SiO_2 nanocatalysts, with the latter being moderately more active. In contrast, substrates with bulkier moieties yielded less product due to steric hindrance slightly impeding the cycloaddition process (Table 3, entries 6–8).

To evaluate the heterogeneity of the nanocatalysts, a simple experiment was conducted to determine whether the reaction took place on the solid surface of the catalyst or whether it was catalyzed by silver metal that might have leached into the liquid phase. Initially, a typical reaction was performed using phenyl nitrile, and, after 3 hours, the reaction was paused, and the conversion was calculated to be 48%. The catalyst was then separated by centrifugation, and the reaction was resumed using the remaining filtrate for an additional two hours. However, the conversion of phenyl nitrile remained unchanged, indicating no further progress in the reaction. Furthermore, ICP-OES analysis of the filtrate revealed no traces of silver. These investigations strongly suggest that only silver attached to the support was active, and that the reaction occurred solely on the catalyst surface.

Table 3 Synthesis of 5-Substituted 1*H*-Tetrazoles using GA-Ag-TiO_2 and GA-Ag-SiO_2 Nanocomposites[a]

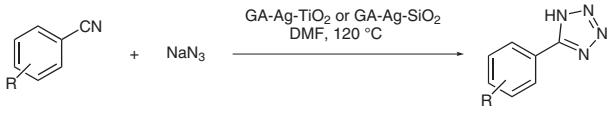

Entry	Substrate	Product	Time (h)[b]	Yield (%)[c]
1	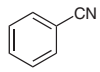	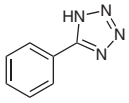	5 (5)	84 (87)
2	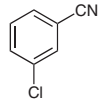	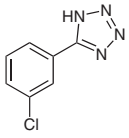	5 (5)	72 (76)
3	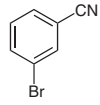	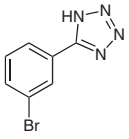	5 (5)	82 (84)
4	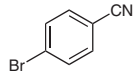	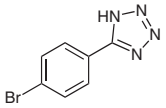	5 (5)	84 (86)
5	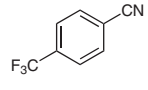	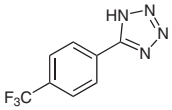	6 (6)	71 (74)
6	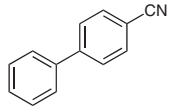	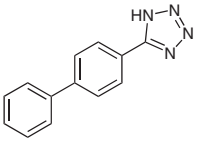	6 (6)	65 (67)
7	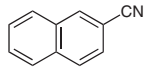	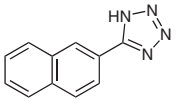	6 (6)	72 (75)
8	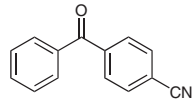	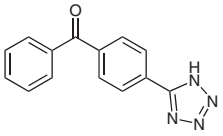	6 (6)	69 (74)

[a] Reaction conditions: phenyl nitrile (1 mmol), NaN_3 (1.5 mmol) in DMF at 120 °C, catalyst (100 mg).
[b] Reaction time using GA-Ag-TiO_2; reaction time using GA-Ag-SiO_2 in parentheses.
[c] Yield using GA-Ag-TiO_2; yield using GA-Ag-SiO_2 in parentheses.

Reuse of Catalyst

To demonstrate the recycling efficacy of the nanocatalysts, the catalyst was removed from the reaction mixture through centrifugation at the conclusion of a reaction, thoroughly washed with ethyl acetate, dried, and then reused in subsequent cycles. Remarkably, the catalysts were effectively utilized for up to five cycles without any signs of activity loss (Table 4). These findings are well-supported by TEM images (see the Supporting Information), which confirm consistent size and shape of the nanocatalysts after five cycles. This can be attributed to the stabilization of silver nanoparticles along with TiO_2 or SiO_2 nanoparticles by the gum acacia matrix. Furthermore, the synergistic effect of TiO_2 or SiO_2 not only prevented silver nanoparticles from coalescing but also enhanced the overall durability and subsequent catalytic performance of the nanocatalysts.

Table 4 Recycling of GA-Ag-TiO_2 and GA-Ag-SiO_2 for the Synthesis of 5-Phenyl-1*H*-tetrazole[a]

Entry	Catalyst	Cycle (% yield)					Average yield (%)
		1	2	3	4	5	
1	GA-Ag/TiO_2	84	83	82	81	79	82
2	GA-Ag/SiO_2	87	87	86	85	84	86

[a] Reaction conditions: Catalyst (100 mg), phenylnitrile (1 mmol), NaN_3 (1.5 mmol) in DMF at 120 °C for 5 h.

Conclusion

We have presented bio-directed and sustainable gum acacia stabilized Ag-SiO_2 and Ag-TiO_2 nanohybrid catalytic systems for the in-situ [3+2] cycloaddition of aryl nitriles and sodium azide. Both catalysts demonstrated excellent performance under the given reaction conditions, resulting in satisfactory yields. Notably, the as-synthesized catalysts exhibited high recycling efficacy and chemical stability. The main advantages of this approach include excellent selectivity of the catalytic system, an easy work-up procedure, low catalytic load, short reaction times, and limited use of toxic reagents during the synthesis process. These factors contribute to the overall sustainability and environmental friendliness of the proposed catalytic systems.

All the chemicals were of analytical quality and were acquired from Sigma Aldrich, St. Louis MO, USA.

Preparation and Evaluation of Catalyst

To prepare GA-Ag-TiO_2, titanium tetraisopropoxide (1 mmol) was homogenized with a 1% gum acacia aqueous solution, and TiO_2 was then precipitated by using a 0.1 M NaOH solution. A stock solution of $AgNO_3$ (0.169 g) in distilled water (100 mL) was prepared, and 10 mL

of this solution was carefully added to the above homogenized mixture under continuous stirring. The resulting solution was transferred to a Teflon-coated stainless-steel vial and subjected to hydrothermal treatment at 150 °C for 6 hours. After centrifugation of the solution, the grey powder thus obtained was thoroughly washed with EtOH and acetone, and finally dried in an oven for 8 hours at 100 °C.

GA-Ag-SiO_2 was prepared likewise with tetraethyl orthosilicate as the precursor.

For the evaluation of catalytic activity, initially, aryl nitrile (1.0 mmol) and GA-Ag-TiO_2 or GA-Ag-SiO_2 nanocatalyst (100 mg) were stirred in DMF (3 mL) for 10–15 minutes at room temperature. NaN_3 (1.5 mmol) was slowly introduced to this mixture, and the reaction temperature was set to 120 °C for 5 hours. The progress of the reaction was continuously tracked using TLC. Once the reaction was completed, the reaction mixture was allowed to cool. The catalyst was separated by centrifugation, washed twice with EtOAc, and then dried in an oven for use in the next cycle.

The reaction mixture was acidified to pH 2 using dilute HCl solution. After separating the supernatant organic layer, the resultant aqueous layer was extracted with EtOAc. After careful evaporation of solvent under reduced pressure, the crude product was subjected to crystallization with 60% EtOAc in hexane to yield pure 5-substituted 1*H*-tetrazole. The spectroscopic data of all the synthesized products were consistent with published data.

5-Phenyl-1*H*-tetrazole (Table 3, entry 1)[76]

Yield: 84% (0.122 g; 0.836 mmol) with GA-Ag-TiO_2 and 87% (0.127 g; 0.870 mmol) with GA-Ag-SiO_2; white solid; mp 212–215 °C (Lit. 215–216 °C).

^{1}HNMR (300 MHz, $CDCl_3$ + DMSO-d_6): δ = 8.03–8.09 (m, 2 H), 7.45–7.55 (m, 3 H).

^{13}CNMR (75 MHz, $CDCl_3$ + DMSO-d_6): δ = 155.05, 130.22, 128.32, 126.34, 123.67.

5-(3-Chlorophenyl)-1*H*-tetrazole (Table 3, entry 2)[77]

Yield: 72% (0.130 g; 0.720 mmol) with GA-Ag-TiO_2 and 76% (0.137 g; 0.759 mmol) with GA-Ag-SiO_2; white solid; mp 138–139 °C (Lit. 139–140 °C).

^{1}HNMR (300 MHz, $CDCl_3$ + DMSO-d_6): δ = 8.10 (s, 1 H), 7.99–8.04 (m, 1 H), 7.44–7.55 (m, 2 H).

^{13}CNMR (75 MHz, $CDCl_3$ + DMSO-d_6): δ = 154.75, 133.88, 129.88, 129.73, 126.14, 125.76, 124.47.

5-(3-Bromophenyl)-1*H*-tetrazole (Table 3, entry 3)[78]

Yield: 82% (0.184 g; 0.818 mmol) with GA-Ag-TiO_2 and 84% (0.189 g; 0.840 mmol) with GA-Ag-SiO_2; white solid; mp 155–156 °C (Lit. 154–155 °C).

^{1}HNMR (300 MHz, $CDCl_3$ + DMSO-d_6): δ = 8.26 (s, 1 H), 8.06 (d, *J* = 7.74 Hz, 1 H), 7.64 (d, *J* = 7.9 Hz, 1 H), 7.40–7.48 (m, 1 H).

^{13}CNMR (75 MHz, $CDCl_3$ + DMSO-d_6): δ = 154.55, 132.67, 129.86, 128.93, 126.00, 124.82, 121.88.

5-(4-Bromophenyl)-1*H*-tetrazole (Table 3, entry 4)[77]

Yield: 84% (0.189 g; 0.840 mmol) with GA-Ag-TiO_2 and 86% (0.193 g; 0.858 mmol) with GA-Ag-SiO_2; white solid; mp 266–268 °C (Lit. 268–269 °C).

^{1}HNMR (300 MHz, $CDCl_3$ + DMSO-d_6): δ = 7.99 (d, *J* = 8.49 Hz, 2 H), 7.67 (d, *J* = 8.49 Hz, 2 H).

^{13}CNMR (75 MHz, $CDCl_3$ + DMSO-d_6): δ = 153.58, 130.55, 127.03, 123.03, 122.08.

5-[4-(Trifluoromethyl)phenyl]-1*H*-tetrazole (Table 3, entry 5)[56]

Yield: 71% (0.152 g; 0.710 mmol) with GA-Ag-TiO_2 and 74% (0.158 g; 0.738 mmol) with GA-Ag-SiO_2; white solid; mp 222–224 °C (Lit. 224–226 °C).

^{1}H NMR (300 MHz, $CDCl_3$ + DMSO-d_6): δ = 8.27 (d, *J* = 7.93 Hz, 2 H), 7.81 (d, *J* = 7.74 Hz, 2 H).

^{13}C NMR (75 MHz, $CDCl_3$ + DMSO-d_6): δ = 154.90, 131.06 (q, *J* = 32.46 Hz), 127.69, 126.57, 124.95 (q, *J* = 3.30 Hz), 124.49.

5-(Biphenyl-4-yl)-1*H*-tetrazole (Table 3, entry 6)[57]

Yield: 65% (0.144 g; 0.648 mmol) with GA-Ag-TiO_2 and 67% (0.149 g; 0.670 mmol) with GA-Ag-SiO_2; white solid; mp 247–250 °C (Lit. 247–249 °C).

^{1}HNMR (300 MHz, $CDCl_3$ + DMSO-d_6): δ = 7.99 (d, *J* = 8.49 Hz, 2 H), 7.67 (d, *J* = 8.49, 2 H).

^{13}CNMR (75 MHz, $CDCl_3$ + DMSO-d_6): δ = 160.62, 154.0, 141.60, 138.0, 127.40, 126.44, 126.01, 125.36, 121.96.

5-Naphthalen-2-yl-1*H*-tetrazole (Table 3, entry 7)[57]

Yield: 72% (0.141 g; 0.719 mmol) with GA-Ag-TiO_2 and 75% (0.149 g; 0.759 mmol) with GA-Ag-SiO_2; white solid; mp 204–206 °C (Lit. 205–207 °C).

^{1}H NMR (300 MHz, $CDCl_3$ + DMSO-d_6): δ = 8.74 (d, *J* = 7.9 Hz, 1 H), 7.9–8.09 (m, 3 H), 7.52–7.66 (m, 3 H).

^{13}CNMR (75 MHz, $CDCl_3$ + DMSO-d_6): δ = 154.22, 132.15, 129.93, 128.87, 127.04, 126.78, 126.04, 125.16, 123.97, 123.63, 120.36.

[4-(1*H*-Tetrazol-5-yl) phenyl](phenyl)methanone (Table 3, entry 8)[57]

Yield: 69% (0.173 g; 0.692 mmol) with GA-Ag-TiO_2 and 64% (0.160 g; 0.639 mmol) with GA-Ag-SiO_2; white solid; mp 198–199 °C (Lit. 197–199 °C).

^{1}HNMR (300 MHz, $CDCl_3$ + DMSO-d_6): δ = 8.23 (d, *J* = 8.3 Hz, 2 H), 7.9 (d, *J* = 8.3 Hz, 2 H), 7.78 (d, *J* = 8.30 Hz, 2 H), 7.59–7.67 (m, 1 H), 7.48–7.56 (m, 2 H).

^{13}CNMR (75 MHz, $CDCl_3$ + DMSO-d_6): δ = 194.751, 155.35, 138.45, 136.17, 132.02, 129.72, 129.04, 127.65, 126.25.

Conflict of Interest

The authors declare no conflict of interest.

Supporting Information

Supporting information for this article is available online at https://doi.org/10.1055/s-0042-1751511.

References

(1) Mukherjee, S.; Chowdhury, D.; Kotcherlakota, R.; Patra, S.; Vinothkumar, B.; Bhadra, M. P.; Sreedhar, B.; Patra, C. R. *Theranostics* **2014**, *4*, 316.

(2) Mukherjee, S.; Sushma, V.; Patra, S.; Barui, A. K.; Bhadra, M. P.; Sreedhar, B. *Nanotechnology* **2012**, *23*, 455103.
(3) Iravani, S. *Green Chem.* **2011**, *13*, 2638.
(4) Mukherjee, S.; Vinothkumar, B.; Prashanthi, S.; Bangal, P. R.; Sreedhar, B.; Patra, C. R. *RSC Adv.* **2013**, *3*, 2318.
(5) Chasteen, N. D.; Harrison, P. M. *J. Struct. Biol.* **1999**, *126*, 182.
(6) Shenton, W.; Mann, S.; Colfen, H.; Bacher, A.; Fischer, M. *Angew. Chem. Int. Ed.* **2001**, *40*, 442.
(7) Xie, J.; Lee, J. Y.; Wang, D. I.; Ting, Y. P. *ACS Nano* **2007**, *1*, 429.
(8) Niemeyer, C. M. *Angew. Chem. Int. Ed.* **2001**, *40*, 4128.
(9) Katz, E.; Willner, I. *Angew. Chem. Int. Ed.* **2004**, *43*, 6042.
(10) Murray, C. B.; Kagan, C. R.; Bawendi, M. G. *Annu. Rev. Mater. Sci.* **2000**, *30*, 545.
(11) Verma, A.; Rotello, V. M. *Chem. Commun.* **2005**, *3*, 303.
(12) Wang, J. *Small* **2005**, *1*, 1036.
(13) Huber, D. L. *Small* **2005**, *1*, 482.
(14) Bandyopadhyaya, R.; Nativ-Roth, E.; Regev, O.; Yerushalmi-Rozen, R. *Nano Lett.* **2002**, *2*, 25.
(15) Kattumuri, V.; Katti, K.; Bhaskaran, S.; Boote, E. J.; Casteel, S. W.; Fent, G. M.; Robertson, D. J.; Chandrasekhar, M.; Kannan, R.; Katti, K. V. *Small* **2007**, *3*, 333.
(16) Velikov, K. P.; Zegers, G. E.; Blaaderen, A. V. *Langmuir* **2003**, *19*, 1384.
(17) Zhang, Y.; Shan, G. B.; Liu, H. Z.; Xing, J. M. *Surf. Coat. Technol.* **2007**, *201*, 6917.
(18) Devi, D. K.; Pratap, S. V.; Haritha, R.; Sivudu, K. S.; Radhika, P.; Sreedhar, B. *J. Appl. Polym. Sci.* **2011**, *121*, 1765.
(19) Schauerrrmann, S.; Nilius, N.; Shaikhutdinov, S.; Freund, H.-J. *Acc. Chem. Res.* **2013**, *46*, 1673.
(20) Sheng, W.; Weng, Q. *Curr. Org. Chem.* **2011**, *15*, 3692.
(21) Zaera, F. *Chem. Soc. Rev.* **2013**, *42*, 2746.
(22) Patra, S.; Naik, A. N.; Pandey, A. K.; Sen, D.; Mazumder, S.; Goswami, A. *Appl. Catal., A* **2016**, *524*, 214.
(23) Castle, A. B.; Garcia-Espino, E.; Nieto-Delgado, C.; Terrones, H.; Terrones, M.; Hussain, S. *ACS Nano* **2011**, *5*, 2458.
(24) Salam, N.; Nanerjee, B.; Roy, A. S.; Mondal, P.; Roy, S.; Bhaumik, A.; Islam, Sk. M. *Appl. Catal., A* **2014**, *477*, 184.
(25) Poreddy, R.; Garcia-Suarez, E. J.; Riisager, A.; Kegnaes, S. *Dalton Trans.* **2014**, 4255.
(26) Signori, A. M.; Santos, K. de. O.; Eising, R.; Albuquerque, B. L.; Giacomelli, F. C.; Domingos, J. *Langmuir* **2016**, *22*, 17772.
(27) He, C.; Li, J.; Cheng, J.; Li, L.; Li, P.; Hao, Z.; Xu, Z. P. *Ind. Eng. Chem. Res.* **2009**, *48*, 6930.
(28) Dong, X.-Y.; Gao, Z.-W.; Yang, K.-F.; Zhang, W.-Q.; Xu, L.-W. *Catal. Sci. Technol.* **2015**, *5*, 2554.
(29) Yu, M.; Wang, Y.; Sun, W.; Yao, X. *Adv. Synth. Catal.* **2012**, *354*, 71.
(30) Wang, H.; Yang, K. F.; Li, L.; Bai, Y.; Zheng, Z. J.; Zhang, W. Q.; Gao, Z. W.; Xu, L. W. *ChemCatChem* **2014**, *6*, 580.
(31) Mohammadi, R.; Eidi, E.; Ghavami, M.; Kassaee, M. Z. *J. Mol. Catal. A: Chem.* **2014**, *393*, 309.
(32) Mistudome, T.; Matoba, M.; Mizugaki, T.; Jitsukawa, K.; Kaneda, K. *Chem. Eur. J.* **2013**, *19*, 5255.
(33) Li, L.; Niu, Z.; Cai, S.; Zhi, Y.; Li, H.; Rong, H.; Liu, L.; He, W.; Li, Y. *Chem. Commun.* **2013**, *49*, 6843.
(34) Cai, S.; Rong, H.; Yu, X.; Liu, X.; Wang, D.; He, W.; Li, Y. *ACS Catal.* **2013**, *3*, 478.
(35) Anandhakumar, S.; Sasidharan, M.; Tsao, C. W.; Raichur, A. M. *ACS Appl. Mater. Interfaces* **2014**, *6*, 3275.
(36) Yasukawa, T.; Miyamura, H.; Kobayashi, S. *J. Am. Chem. Soc.* **2012**, *134*, 16963.
(37) Butler, R. N. *Comprehensive Heterocyclic Chemistry, Vol. 2*; Pergamon: Oxford, **1996**, 621.
(38) Herr, R. J. *Bioorg. Med. Chem.* **2002**, *10*, 3379.
(39) Larock, R. C. *Comprehensive Organic Transformations: A Guide to Functional Group Preparations*; VCH Publishers: New York, **1989**.
(40) Myznikov, L. V.; Hrabalek, A.; Koldobskii, G. I. *Chem. Heterocycl. Compd.* **2007**, *43*, 1.
(41) Kumar, C. N. S. S. P.; Parida, D. K.; Santhoshi, A.; Kota, A. K.; Sridhar, B.; Rao, V. J. *MedChemComm* **2011**, *2*, 486.
(42) Malik, M. A.; Al-Thabaiti, S. A.; Malik, M. A. *Int. J. Mol. Sci.* **2012**, *13*, 10880.
(43) Disli, A.; Mercan, S.; Yavuz, S. *J. Heterocycl. Chem.* **2013**, *50*, 1446.
(44) *Progress in Medicinal Chemistry*; Ellis, E. P.; West, G. B., Ed.; Biomedical Press: North Holland, **1980**.
(45) Yavuz, S.; Unal, Y.; Pamir, O.; Yilmazer, D.; Kurtipek, O.; Kavutcu, M.; Arslan, M.; Ark, M.; Yildirir, Y. *Arch. Pharm. Chem. Life Sci.* **2013**, *346*, 455.
(46) Jursic, B. S.; Leblanc, B. W. J. *J. Heterocycl. Chem.* **1998**, *35*, 405; and references cited therein.
(47) Sandmann, G.; Schneider, C.; Boger, P. Z.; Naturforsch, C. *Bioscience* **1996**, *51*, 534.
(48) Zhaoxu, C.; Heming, X. *Propellants, Explos., Pyrotech.* **1999**, *24*, 319.
(49) Damayarapu, R.; Klapotke, T. M.; Steirstorfer, J.; Tarantik, K. R. *Propellants, Explos., Pyrotech.* **2010**, *35*, 395.
(50) Frija, L. M. T.; Ismael, A.; Cristiano, M. L. S. *Molecules* **2010**, *15*, 3757.
(51) Jaroslav, R.; Vavrova, K.; Hrabalek, A. *Eur. J. Org. Chem.* **2012**, 6101.
(52) Esirden, I.; Basar, E.; Kaya, M. *Chem. Pap.* **2015**, *69*, 1231.
(53) Bonnamour, J.; Bolm, C. *Chem. Eur. J.* **2009**, *15*, 4543.
(54) Bosch, L.; Vilarrasa, J. *Angew. Chem. Int. Ed.* **2007**, *46*, 3926.
(55) Schmidt, B.; Meid, D.; Keiser, D. *Tetrahedron* **2007**, *63*, 492.
(56) Khalafi-Nezhad, A.; Mohammadi, S. *RSC Adv.* **2013**, *3*, 4362.
(57) Sreedhar, B.; Kumar, A. S.; Yada, D. *Tetrahedron Lett.* **2011**, *52*, 3565.
(58) Dehghani, F.; Sardarian, A. R.; Esmaeilpour, M. *J. Organomet. Chem.* **2013**, *743*, 87.
(59) Swami, S.; Sahu, S. N.; Shrivatsava, R. *RSC Adv.* **2021**, *11*, 39058.
(60) Mani, P.; Sharma, C.; Kumar, S.; Awasthi, S. K. *J. Mol. Catal. A: Chem.* **2014**, *392*, 150.
(61) Feng, S.; Wang, M.; Zhou, Y.; Li, P.; Tu, W.; Zou, Z. *APL Materials* **2015**, *3*, 104416.
(62) Wu, H.; Huang, J.; Liu, Y. *J. Water Health* **2017**, *15*, 341.
(63) Wang, B.; Zhu, X.; Li, S.; Chen, M.; Lu, H.; Yang, Y. *Nanomaterials* **2018**, *8*, 701.
(64) Khan, M. M.; Ansari, S. A.; Amal, M. I.; Lee, J.; Cho, M. H. *Nanoscale* **2013**, *5*, 4427.
(65) Sreedhar, B.; Vani, C. S.; Devi, D. K.; Rao, M. V. B.; Rambabu, C. *Am. J. Mater. Sci.* **2012**, *2*, 5.
(66) Sreedhar, B.; Devi, D. K.; Neetha, A. S.; Kumar, V. P.; Chary, K. V. R. *Mater. Chem. Phys.* **2015**, *153*, 23.
(67) Supriya, P.; Srinivas, B. T. V.; Chowdeswari, K.; Naidu, N. V. S.; Sreedhar, B. *Mater. Chem. Phys.* **2018**, *204*, 27.
(68) Litran, R.; Sampedro, B.; Rojas, T. C.; Multigner, M.; Sanchez-Lapez, J. C.; Crespo, P.; Lopez-Cartes, C.; Garcia, M. A.; Hernando, A.; Fernandez, A. *Phys. Rev. B: Condens. Matter Mater. Phys.* **2006**, *73*, 54404.
(69) NIST X-ray Photoelectron Spectroscopy Database NIST Standard Reference Database 20, Version 3.4. June 06, 2000; http://srdata.nist.gov/xps/

(70) Nasrollahzadeh, M.; Sajadi, S. M.; Rostami-Vartooni, A.; Alizadeh, M.; Bagherzadeh, M. *J. Colloid Interface Sci.* **2016**, *466*, 360.
(71) Ganapathy, M.; Senthilkumar, N.; Vimalan, M.; Jeysekaran, R.; Potheher, I. V. *Mater. Res. Express* **2018**, *5*, 45020.
(72) Ramalingam, S.; Devi, L. B.; Rao, J. R.; Nair, B. U. *RSC Adv.* **2014**, *4*, 56041.
(73) Hosseini-Sarvari, M.; Najafvand-Derikvandi, S. *C. R. Chim.* **2014**, *17*, 1007.
(74) Patil, U. B.; Kumthekar, K. R.; Nagarkar, J. M. *Tetrahedron* **2012**, *53*, 3706.
(75) Mani, P.; Singh, A. K.; Awasthi, S. K. *Tetrahedron Lett.* **2014**, *55*, 1879.
(76) Cantillo, D.; Gutmann, B.; Kappe, C. O. *J. Org. Chem.* **2012**, *77*, 10882.
(77) Patil, D. R.; Wagh, Y. B.; Ingole, P. G.; Singh, K.; Dalal, D. S. *New J. Chem.* **2013**, *37*, 3261.
(78) Sharghi, H.; Ebrahimpourmoghaddam, S.; Doroodmand, M. M. *J. Organomet. Chem.* **2013**, *738*, 41.